International Journal of Scientific Engineering and Research (IJSER)
ISSN (Online): 2347-3878
Index Copernicus Value (2015): 62.86 | Impact Factor (2015): 3.791

Investigation of Graphene Optoelectronic Properties in Sub-100 THz Band

Mustafa M. A. Abdulqader[1], Raad S. Fyath[2]

[1]Department of Laser and Optoelectronics Engineering, Al Nahrain University,
Baghdad, Iraq
mmaj2013fma[at]gmail.com

[2]Department of Computer Engineering, Al Nahrain University,
Baghdad, Iraq
Rsfyath[at]yahoo.com

Abstract: ***This paper investigates the optoelectronic properties of graphene operating in the 0.1 – 100 THz frequency band. The graphene surface conductivity is calculated using Kubo formula and the results used to calculate the complex relative permittivity and the complex refractive index. The calculated results reveal that the real parts of the interband and intraband components of graphene surface conductivity becomes equal at certain frequency, f_{cross}, which is an increasing function of chemical potential μ_c. Operating above f_{cross} makes the contribution of the interband component higher than the contribution of the intraband component. At μ_c = 0.1 and 0.2 eV, f_{cross} is equal 21.7 and 54.4 Thz, respectively.***

Keywords: Graphene, Terahertz, Mathematical Modeling, and Conductivity.

1. Introduction

Graphene has attracted tremendous interests due to its unique optical and electrical properties [1]–[4]. Graphene is a two-dimensional (2D) single carbon-atom layer where electrons and holes hold a linear dispersion relation with zero bandgap [5]. Graphene technology has been applied successfully to produce compact, efficient and frequency-tunable devices operating at optical telecommunication wavelength [6]–[9] and terahertz (THz) radiation band. The frequency-tunablity of graphene comes from the dependence of its optoelectronic properties on the applied voltage [10], [11]. In THz region, graphene material has been investigated comprehensively in the literature for various applications such as antennas [12]–[15], modulators [16], [17], generation and detection [5], [18], [19], wireless communications [20], [21], and nano communications [22]–[24].

The optoelectronic properties of graphene have been investigated in the literature for visible optical regime [25], optical telecommunication wavelengths (1310 and 1550 nm) [4], [26]–[28], and for below 10 THz band [29]–[31]. The analysis and results reported in these papers stand on Kubo formula which splits the graphene surface conductivity into two components due to intraband an interband transitions [32]–[34].

The aim of this paper is to predict the optoelectronic properties of graphene material operating in deep THz regime (toward 100 THz). This frequency band is expected to be useful for next THz applications especially in the fields of sensing and molecule communications. The Kubo formula is used in this paper to predict the graphene surface conductivity as a function of both frequency and chemical potential. The results are used as a framework to obtain the refractive index and relative permittivity of graphene operating in deep THz band.

2. Mathematical Modeling of Graphene Optoelectronic Properties

Graphene is a 2D material whose electronic band structure contains six Dirac points describing the transition between valence (hole) band and conduction (free electron) band (see Fig. 1a). The energy band has no gap since conical hole and electron bands touch at the Dirac points where the effective carrier density is zero. Therefore, it is expected that both intraband and interband transitions play key role in determining the graphene optoelectronic characteristics (see Fig. 1b).

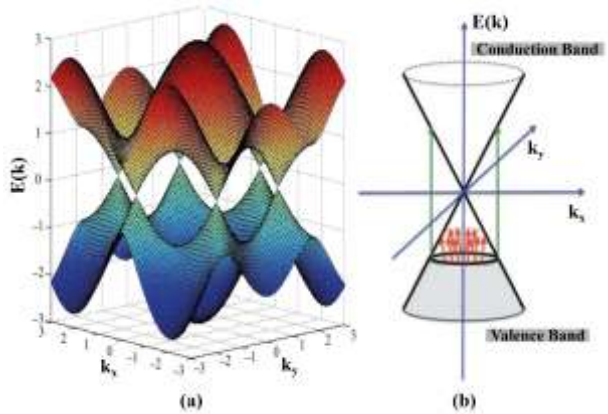

Figure 1: (a) Graphene conduction and valance bands [35]. (b) Intraband and interband transitions (Here, green arrows for interband transitions and red arrows for intraband transitions) [36]. E(k) represents the energy as a function momentum (k).

It is assumed here that the graphene material is implemented as a two-dimensional material on a dielectric substrate, namely SiO_2.The graphene surface conductivity σ_g comes mainly from two contributions, σ_{intra} and σ_{inter} due to intraband and interband transitions, respectively

$$\sigma_g(\omega) = \sigma_{intra}(\omega) + \sigma_{inter}(\omega) \quad (1)$$

where ω is the operating radian frequency. Both surface conductivity components are complex quantities whose frequency dependence is governed by Kubo formula [32]–[34]

$$\sigma_{intra}(\omega) = \frac{q^2 k_B T}{\pi \hbar^2}\left[\frac{\mu_c}{k_B T} + 2\ln(e^{\frac{\mu_c}{k_B T}} + 1)\right]\frac{j}{\omega + j\tau^{-1}} \quad (2a)$$

$$\sigma_{inter}(\omega) = \frac{q^2}{4\pi}\left[H(\omega/2) + j\frac{4\omega}{\pi}\int_0^\infty \frac{H(\grave{\omega}) - H(\omega/2)}{\omega^2 + 4\grave{\omega}^2} d\grave{\omega}\right] \quad (2b)$$

where

$$H(\omega) = \frac{\sinh(\hbar\omega/k_B T)}{\cosh(\mu_c/k_B T) + \cosh(\hbar\omega/k_B T)} \quad (2c)$$

Here q is the electronic charge, k_B is Boltzmann's constant, T is the absolute temperature, and $\hbar$ is reduced Plank's constant. Further, τ is the graphene relaxation time which is the time required for a charge distortion to relax to a uniform charge density after it has been introduced in the graphene, and μ_c is the chemical potential which depends on the applied voltage

$$\mu_c = \hbar v_F \sqrt{\eta\pi\left|V_g - V_{Dirac}\right|} \quad (3)$$

In Eq. 3, V_g is the applied gate voltage, V_{Dirac} is Dirac voltage which is a voltage offset caused by natural doping and estimated to be 0.8 V, v_F is Fermi velocity which is equal to 10^6 m/s, and $\eta = \varepsilon_0\varepsilon_r / qd$ where ε_0 is the vacuum permittivity, ε_r is the relative permittivity of the substrate and d is the substrate layer thickness.

The real and imaginary parts of graphene surface conductivity, σ_{gr} and σ_{gi}, can be expressed as follows

$$\sigma_g(\omega) = \sigma_{gr}(\omega) + j\sigma_{gi}(\omega) \quad (4a)$$

$$\sigma_{gr}(\omega) = \mathrm{Re}\left[\sigma_{intra}(\omega)\right] + \mathrm{Re}\left[\sigma_{inter}(\omega)\right] \quad (4b)$$

$$\sigma_{gi}(\omega) = \mathrm{Im}\left[\sigma_{intra}(\omega)\right] + \mathrm{Im}\left[\sigma_{inter}(\omega)\right] \quad (4c)$$

where Re[•] and Im[•] stand, respectively, for the real and imaginary parts of the argument. Further, using Eqs. 2a-c yields

$$\mathrm{Re}[\sigma_{intra}(\omega)] = Q(\mu_c)\frac{\tau}{\omega^2\tau^2 + 1} \quad (5a)$$

$$\mathrm{Im}[\sigma_{intra}(\omega)] = Q(\mu_c)\frac{\omega\tau^2}{\omega^2\tau^2 + 1} \quad (5b)$$

$$\mathrm{Re}[\sigma_{inter}(\omega)] = \frac{q^2}{4\pi}H(\omega/2) \quad (5c)$$

$$\mathrm{Im}[\sigma_{inter}(\omega)] = \frac{q^2\omega}{\pi^2}\int_0^\infty \frac{H(\grave{\omega}) - H(\omega/2)}{\omega^2 + 4\grave{\omega}^2} d\grave{\omega} \quad (5d)$$

$$Q(\mu_c) = \frac{q^2 k_B T}{\pi\hbar^2}\left[\frac{\mu_c}{k_B T} + 2\ln(e^{\frac{\mu_c}{k_B T}} + 1)\right] \quad (5e)$$

Few remarks regarding the above formulation are given here

i. The effect of chemical potential μ_c becomes negligible when its value is much less than the thermal equivalent voltage $V_{Th}=k_B T$. At room temperature, V_{Th} is about 26 meV. Thus the chemical potential play a key role in determining the optoelectronic properties of graphene when it is subjected to applied voltage.
ii. Both the real and imaginary parts of $\sigma_{inter}(\omega)$ depend on the chemical potential and this dependence comes from the definition of H(ω).

The graphene relative permittivity $\varepsilon_g(\omega)$ is related to the surface conductivity by

$$\varepsilon_g(\omega) = 1 + j\frac{\sigma_g(\omega)}{\omega\varepsilon_0 t_g} \quad (6)$$

where t_g is the thickness of the graphene layer.

The real and imaginary parts, ε_{gr} and ε_{gi}, of the graphene relative permittivity can be expressed as

$$\varepsilon_{gr}(\omega) = 1 - \frac{\sigma_{gi}(\omega)}{\omega\varepsilon_0 t_g} \quad (7a)$$

$$\varepsilon_{gi}(\omega) = \frac{\sigma_{gr}(\omega)}{\omega\varepsilon_0 t_g} \quad (7b)$$

The graphene refractive index $n_g(\omega)$ can be expressed as the square root of the graphene relative permittivity

$$n_g(\omega) = \sqrt{\varepsilon_g(\omega)} \quad (8)$$

The parameter $n_g(\omega)$ can be expressed as

$$n_g(\omega) = n_{gr}(\omega) + jn_{gi}(\omega) \quad (9a)$$

where the real part $n_{gr}(\omega)$ and the imaginary part $n_{gi}(\omega)$ are computed, respectively, from

$$n_{gr}(\omega) = \left|n_g(\omega)\right|\cos\phi_{ng}(\omega) \quad (9b)$$

$$n_{gi}(\omega) = \left|n_g(\omega)\right|\sin\phi_{ng}(\omega) \quad (9c)$$

where

$$\left|n_g(\omega)\right| = \left[1 - \frac{2\sigma_{gi}(\omega)}{\omega\varepsilon_0 t_g} + \frac{\sigma_{gr}^2(\omega) + \sigma_{gi}^2(\omega)}{(\omega\varepsilon_0 t_g)^2}\right]^{\frac{1}{2}} \quad (9d)$$

$$\phi_{ng}(\omega) = \frac{1}{2}\tan^{-1}\left[\frac{\sigma_{gr}(\omega)}{1 - \frac{\sigma_{gr}(\omega)}{\omega\varepsilon_0 t_g}}\right] \quad (9e)$$

3. Numerical Results

This section presents numerical results characterizing graphene surface conductivity, relative permittivity, and complex refractive index over a frequency band up to 100 THz. Unless otherwise stated, the graphene optoelectronic properties are obtained at room temperature using the following parameters values: relaxation time $\tau = 10^{-13}$ s and graphene thickness $t_g = 0.335$ nm.

3.1 Surface Conductivity

Figs. 2(a-c) show the variation of the real part of graphene surface conductivity, Re[σ_g], with the operating frequency for a chemical potential of 0, 0.5 and 1 eV, respectively. Both interband and intraband contributions to Re[σ_g] are included in these figures. Investigating the results in these figures highlights the following fact

i. The intraband component is a decreasing function of frequency while the interband component is an increasing function of frequency.
ii. Increasing the chemical potential μ_c leads to higher (lower) contribution of intraband (interband) component.
iii. At μ_c = 0 eV, the contributions of interband and intraband transitions to Re[σ_g] are equal at f = 7.45 THz;(This frequency is denoted here by f_{cross}). This leads to a minimum value of Re[σ_g] equals 36 uS at this frequency.
iv. Incresing μ_c will push f_{cross} to higher frequency and make the contribution of interband transitions almost negligible in the 100 THz band.

The dependence of cross over frequency f_{cross} on the chemical potential is calculated and the results are depicted in Fig. 3. Note that f_{cross} = 100 THz occurs when μ_c approaches 0.31 eV.

The spectral behavior of the imaginary part of graphene surface conductivity, Im[σ_g], is also calculated and the results are given in Fig. 4. Parts a, b, and c of this figure corresponds to μ_c =0, 0.5, and 1 eV, respectively. Investigating the results depicted in this figure reveals the following findings

i. The effect of interband component is almost negligible and this effect is more pronounced with increasing μ_c.
ii. At fixed value of frequency, increasing the chemical potential leads to higher values of Im[σ_g].
iii. The intraband component (and hence the total value) of Im[σ_g] approaches a maximum value at certain frequency, f_{max}. The value of f_{max} is approximately 1.6 THz and it is independent on μ_c. The corresponding values of Im[σ_g] are 0.211, 2.943 and 5.886 mS at μ_c = 0, 0.5 and 1 eV, respectively.

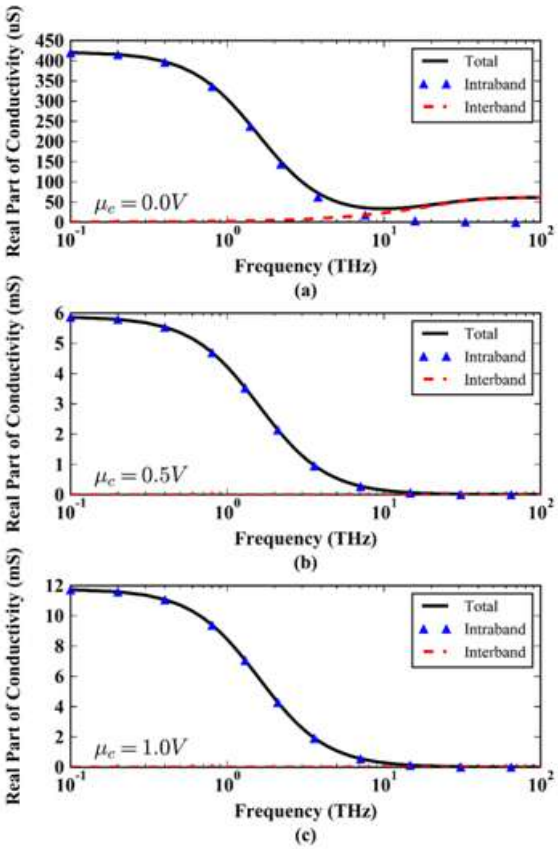

Figure 2: Variation of real part of graphene surface conductivity with frequency. (a) μ_c = 0 eV (b) μ_c = 0.5 eV (c) μ_c = 1 eV

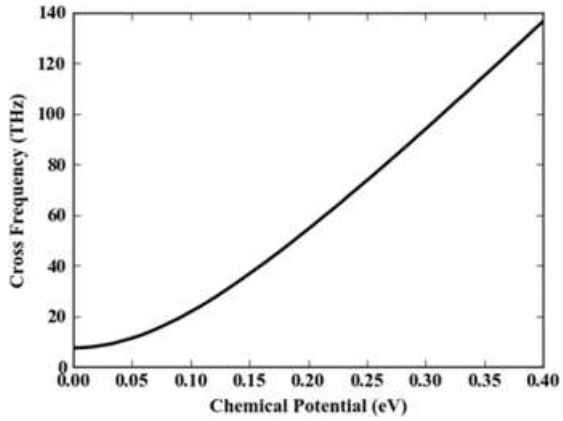

Figure 3: Dependence of the cross frequency f_{cross} on the chemical potential.

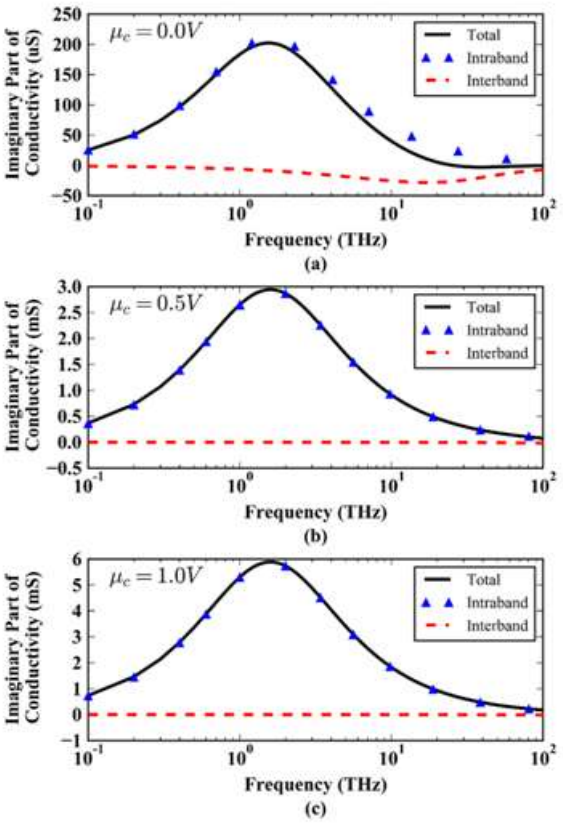

Figure 4: Variation of imaginary part of graphene surface conductivity with frequency. (a) μ_c = 0 eV (b) μ_c = 0.5 eV (c) μ_c = 1 eV

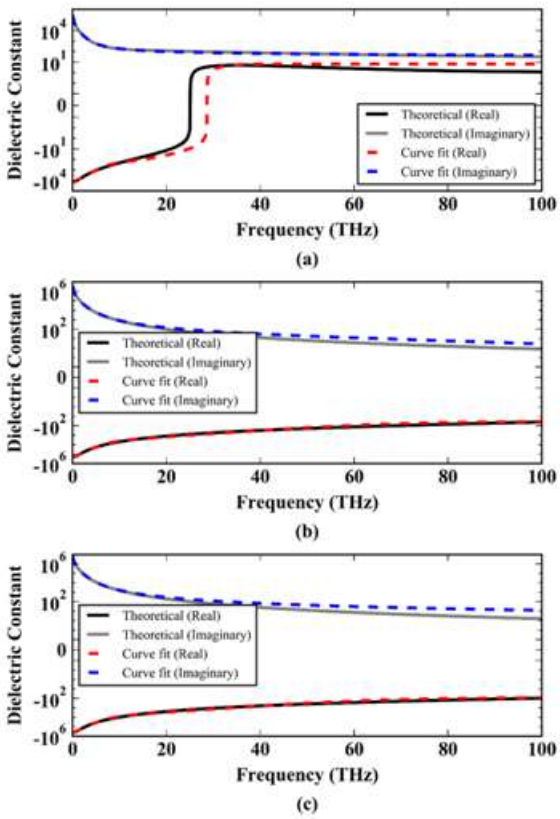

Figure 5: Frequency spectra of graphene dielectric constant for different values of chemical potential µc. Dashed curves correspond to curve fitting. (a) μ_c = 0 eV (b) μ_c = 0.5 eV (c) μ_c = 1 eV

3.2 Dielectric Constant and Refractive Index

The spectral behavior of the dielectric constant (relative permittivity) of graphene ε_g is given in Figs. 5(a-c) for μ_c = 0, 0.5 and 1 eV, respectively. For comparison purposes, both real and imaginary parts of ε_g are displayed in these figures. The dashed curves in these figures are obtained after applying curve fitting (see appendix A). Note that Re[ε_g] is negative at μ_c = 0.5 and 1 eV.

The dependence of the real and imaginary parts of the dielectric constant on chemical potential is displayed in Fig. 6 for different values of operating frequency. It is worth to notice here that at f = 1 and 10 THz, The real (imaginary) part of ε_g decreases (increases) almost linearly with μ_c. At f = 50 and 100 THz, the linear dependence of ε_g parts on μ_c is not valid and the Re[ε_g] becomes positive at low values of μ_c.

The calculations are carried further to investigate the frequency dependence of graphene refractive index n_g and the results are displayed in Fig. 7. Both real and imaginary parts of n_g are presented in this figure for three values of μ_c (0, 0.5, 1 eV). Note that both Re[n_g] and Im[n_g] are positive for all values of μ_c and frequency. Note also that Im[n_g] is much higher than Re[n_g] at μ_c = 0.5 and 1 eV. In contrast, at μ_c = 0 eV, the imaginary part of n_g is higher than the real part over the frequency band below 20 THz. Above 20 THz, both real and imaginary parts of n_g are almost equal.

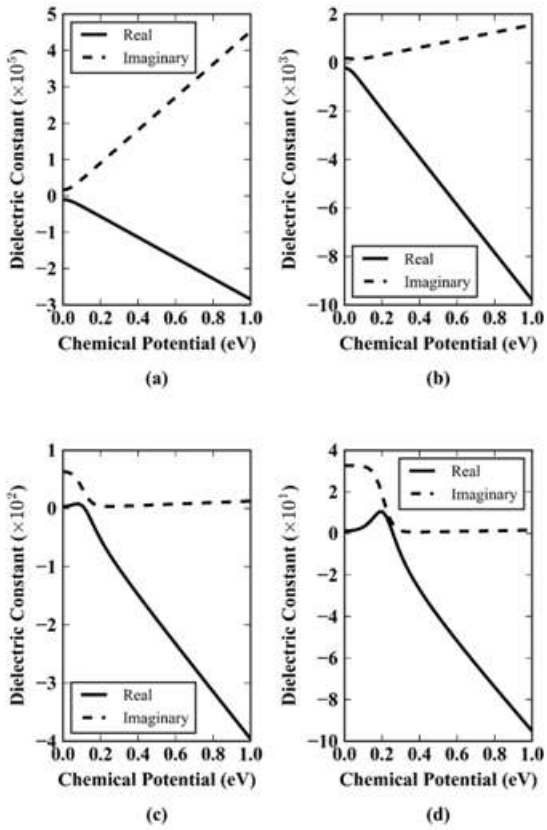

Figure 6: Dependence of real and imaginary parts of graphene dielectric constant on chemical potential. (a) f = 1 THz (b) f = 10 THz (c) f = 50 THz (d) f = 100 THz.

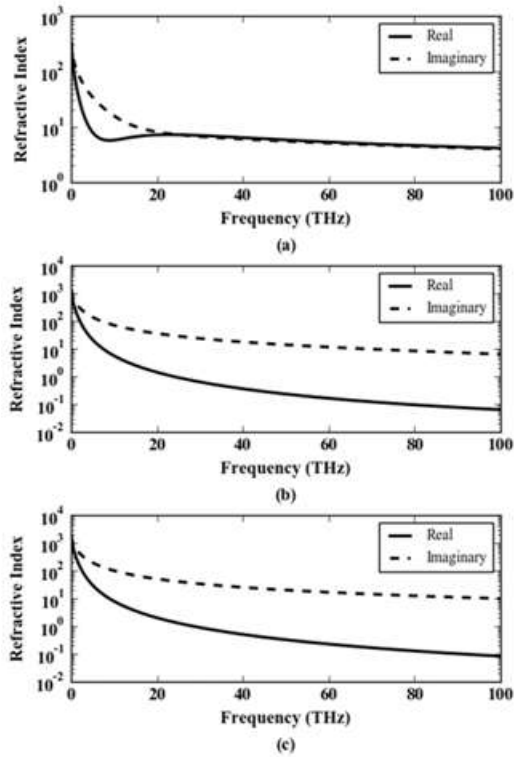

Figure 7: Dependence of real and imaginary parts of graphene dielectric constant on chemical potential. (a) $\mu_c = 0$ eV (b) $\mu_c = 0.5$ eV (c) $\mu_c = 1$ eV.

3.3 Summarized Tables

Tables 1 and 2 list the calculated graphene relative permittivity ε_g and refractive index n_g for different values of chemical potential and operating frequencies. These tables can be used as a basis to investigate the performance of graphene-based devices using commercial software packages.

Table 1: Real and imaginary parts of graphene relative permittivity for various values of chemical potential and operating frequencies.

Chemical Potential (eV)	Relative Permittivity			
	1 THz	10 THz	50 THz	100 THz
0	$-9.857\times10^{3}+j1.636\times10^{4}$	$-2.140\times10^{2}+j1.800\times10^{2}$	$3.417\times10^{0}+j6.341\times10^{1}$	$1.192\times10^{0}+j3.269\times10^{1}$
0.1	$-2.868\times10^{4}+j4.578\times10^{4}$	$-9.323\times10^{2}+j1.692\times10^{2}$	$5.659\times10^{0}+j3.606\times10^{1}$	$3.050\times10^{0}+j3.230\times10^{1}$
0.2	$-5.689\times10^{4}+j9.058\times10^{4}$	$-1.937\times10^{3}+j3.124\times10^{2}$	$-5.288\times10^{1}+j4.077\times10^{0}$	$1.063\times10^{1}+j1.878\times10^{1}$
0.3	$-8.534\times10^{4}+j1.359\times10^{5}$	$-2.926\times10^{3}+j4.681\times10^{2}$	$-1.040\times10^{2}+j3.868\times10^{0}$	$-1.005\times10^{1}+j1.343\times10^{0}$
0.4	$-1.138\times10^{5}+j1.811\times10^{5}$	$-3.910\times10^{3}+j6.242\times10^{2}$	$-1.485\times10^{2}+j5.115\times10^{0}$	$-2.698\times10^{1}+j6.583\times10^{-1}$
0.5	$-1.423\times10^{5}+j2.264\times10^{5}$	$-4.892\times10^{3}+j7.802\times10^{2}$	$-1.910\times10^{2}+j6.393\times10^{0}$	$-3.999\times101+j8.001\times10^{-1}$
0.6	$-1.707\times10^{5}+j2.717\times10^{5}$	$-5.874\times10^{3}+j9.362\times10^{2}$	$-2.327\times10^{2}+j7.672\times10^{0}$	$-5.177\times101+j9.597\times10^{-1}$
0.7	$-1.992\times10^{5}+j3.170\times10^{5}$	$-6.856\times10^{3}+j1.092\times10^{3}$	$-2.740\times10^{2}+j8.950\times10^{0}$	$-6.299\times10^{1}+j1.120\times10^{0}$
0.8	$-2.276\times10^{5}+j3.623\times10^{5}$	$-7.837\times10^{3}+j1.248\times10^{3}$	$-3.149\times10^{2}+j1.023\times10^{1}$	$-7.388\times10^{1}+j1.280\times10^{0}$
0.9	$-2.561\times10^{5}+j4.076\times10^{5}$	$-8.818\times10^{3}+j1.404\times10^{3}$	$-3.557\times10^{2}+j1.151\times10^{1}$	$-8.457\times10^{1}+j1.440\times10^{0}$
1	$-2.845\times10^{5}+j4.528\times10^{5}$	$-9.799\times10^{3}+j1.560\times10^{3}$	$-3.964\times10^{2}+j1.279\times10^{1}$	$-9.513\times10^{1}+j1.600\times10^{0}$

Table 2: Real and imaginary parts of graphene refractive index for various values of chemical potential and operating frequencies.

Chemical Potential (eV)	Refractive Index			
	1 THz	10 THz	50 THz	100 THz
0	$6.798\times10^{1}+j1.203\times10^{2}$	$5.727\times10^{0}+j1.571\times10^{1}$	$5.785\times10^{0}+j5.481\times10^{0}$	$4.117\times10^{0}+j3.970\times10^{0}$
0.1	$1.126\times10^{2}+j2.034\times10^{2}$	$2.759\times10^{0}+j3.066\times10^{1}$	$4.591\times10^{0}+j3.927\times10^{0}$	$4.213\times10^{0}+j3.833\times10^{0}$
0.2	$1.582\times10^{2}+j2.862\times10^{2}$	$3.538\times10^{0}+j4.415\times10^{1}$	$2.801\times10^{1}+j7.277\times10^{0}$	$4.013\times10^{0}+j2.340\times10^{0}$
0.3	$1.938\times10^{2}+j3.506\times10^{2}$	$4.314\times10^{0}+j5.426\times10^{1}$	$1.896\times10^{-1}+j1.020\times10^{1}$	$2.114\times10^{-1}+j3.178\times10^{0}$
0.4	$2.237\times10^{2}+j4.048\times10^{2}$	$4.975\times10^{0}+j6.273\times10^{1}$	$2.099\times10^{-1}+j1.219\times10^{1}$	$6.337\times10^{-2}+j5.194\times10^{0}$
0.5	$2.501\times10^{2}+j4.526\times10^{2}$	$5.560\times10^{0}+j7.017\times10^{1}$	$2.312\times10^{-1}+j1.382\times10^{1}$	$6.326\times10^{-2}+j6.324\times10^{0}$

0.6	2.740×10^{2} $+j4.958\times10^{2}$	6.088×10^{0} $+j7.689\times10^{1}$	2.514×10^{-1} $+j1.526\times10^{1}$	6.669×10^{-2} $+j7.196\times10^{0}$

Table 2: (Continued).

0.7	2.960×10^{2} $+j5.355\times10^{2}$	6.575×10^{0} $+j8.306\times10^{1}$	2.703×10^{-1} $+j1.655\times10^{1}$	7.054×10^{-2} $+j7.937\times10^{0}$
0.8	3.164×10^{2} $+j5.725\times10^{2}$	7.028×10^{0} $+j8.881\times10^{1}$	2.882×10^{-1} $+j1.775\times10^{1}$	7.443×10^{-2} $+j8.596\times10^{0}$
0.9	3.356×10^{2} $+j6.072\times10^{2}$	7.454×10^{0} $+j9.420\times10^{1}$	3.050×10^{-1} $+j1.886\times10^{1}$	7.827×10^{-2} $+j9.197\times10^{0}$
1	3.538×10^{2} $+j6.401\times10^{2}$	7.857×10^{0} $+j9.930\times10^{1}$	3.211×10^{-1} $+j1.991\times10^{1}$	8.199×10^{-2} $+j9.754\times10^{0}$

4. Conclusions

The graphene surface conductivity, relative permittivity, and refractive index have been investigated over 0.1 – 100 THz frequency band using Kubo formula. The calculated results reveal that the intraband component of the real part of the surface conductivity is a decreasing function of frequency while the interband component is an increasing function of frequency, at μ_c = 0 eV, the contributions of interband and intraband transitions to Re[σ_g] are equal at f = 7.45 THz and leads to a minimum value of Re[σ_g] equals 36 uS at this frequency, the effect of the imaginary part of the interband component is almost negligible and this effect is more pronounced with increasing μ_c, the intraband component (and hence the total value) of Im[σ_g] approaches a maximum value at certain frequency, f_{max}. The value of f_{max} is approximately 1.6 THz and it is independent on μ_c and the corresponding values of Im[σ_g] are 0.211, 2.943 and 5.886 mS at μ_c = 0, 0.5 and 1 eV, respectively, at f = 1 and 10 THz, The real (imaginary) part of ε_g decreases (increases) almost linearly with μ_c and at f = 50 and 100 THz, the linear dependence of ε_g parts on μc is not valid and the Re[ε_g] becomes positive at low values of μ_c, both Re[n_g] and Im[n_g] are positive for all values of μ_c and frequency, Im[n_g] is much higher than Re[n_g] at μ_c = 0.5 and 1 eV, and at μ_c = 0 eV, the imaginary part of n_g is higher than the real part over the frequency band below 20 THz, above 20 THz, both real and imaginary parts of n_g are almost equal.

Appendix A: Curve Fitting for the Real and Imaginary Parts of Graphene Relative Permittivity

The following two equations are used for curve fitting the relation between the real and imaginary parts of the relative permittivity, respectively and the operating frequencies

$$\mathrm{Re}[\varepsilon_g] = a_0 + a_1 e^{-b_1 f} + a_2 e^{-b_2 f} + a_3 e^{-b_3 f} \quad \text{(A1)}$$

$$\mathrm{Im}[\varepsilon_g] = a_0 + a_1 e^{(b_1(f+c_1))^{d_1}} + a_2 e^{(b_2(f+c_2))^{d_2}} \quad \text{(A2)}$$

The curve fitting uses the numerical data estimated on the frequency range (0.1 – 100 THz). The values of the fitting parameters are listed in Tables 3 and 4 for μ_c = 0, 0.5 and 1 eV where f in THz

Table 3: Fitting parameters for the real part of the relative permittivity for three values of chemical potential.

	0 eV	0.5 eV	1 eV
a_0	6.715×10^{0}	-3.456×10^{1}	-8.372×10^{1}
a_1	-5.347×10^{6}	-7.471×10^{3}	-1.455×10^{4}
a_2	1.132×10^{7}	-5.430×10^{4}	-1.494×10^{4}
a_3	-5.992×10^{6}	-1.682×10^{5}	-4.304×10^{5}
b_1(THz^{-1})	3.283×10^{-1}	8.190×10^{-2}	5.606×10^{-1}
b_2(THz^{-1})	3.344×10^{-1}	5.606×10^{-1}	8.190×10^{-2}
b_3(THz^{-1})	3.404×10^{-1}	5.606×10^{-1}	5.606×10^{-1}

Table 4: Fitting parameters for the imaginary part of the relative permittivity for three values of chemical potential.

	0 eV	0.5 eV	1 eV
a_0	2.034×10^{1}	-3.549×10^{0}	1.947×10^{-1}
a_1	3.568×10^{0}	5.180×10^{-17}	4.122×10^{-17}
a_2	1.552×10^{-15}	5.198×10^{-14}	5.741×10^{-14}
b_1(THz^{-1})	9.238×10^{-4}	3.135×10^{-38}	4.415×10^{-39}
b_2(THz^{-1})	7.316×10^{-13}	1.749×10^{-14}	9.205×10^{-15}
c_1(THz)	1.468×10^{-1}	8.684×10^{-2}	8.676×10^{-2}
c_2(THz)	3.040×10^{0}	2.559×10^{0}	2.547×10^{0}
d_1	-2.830×10^{-1}	-4.491×10^{-2}	-4.413×10^{-2}
d_2	-1.421×10^{-1}	-1.235×10^{-1}	-1.213×10^{-1}

References

[1] D. Correas-Serrano, J. S. Gomez-Diaz, A. Alù, and A. Á. Melcón, "Electrically and magnetically biased graphene-based cylindrical waveguides: Analysis and applications as reconfigurable antennas," IEEE Transactions on Terahertz Science and Technology, vol. 5, no. 6, pp. 951–960, Nov. 2015.

[2] E. Dremetsika, B. Dlubak, S.-P. Gorza, C. Ciret, M.-B. Martin, S. Hofmann, P. Seneor, D. Dolfi, S. Massar, P. Emplit, and P. Kockaert, "Measuring the nonlinear refractive index of graphene using the optical Kerr effect method," Optics Letters, vol. 41, no. 14, pp. 3281–3284, Jul. 2016.

[3] N. Liu, G. Cai, L. Ye, and Q. H. Liu, "The Efficient Mixed FEM With the Impedance Transmission Boundary Condition for Graphene Plasmonic Waveguides," IEEE Journal of Lightwave Technology, vol. 34, no. 23, pp. 5363–5370, Dec. 2016.

[4] V. Sorianello, G. De Angelis, T. Cassese, M. Midrio, M. Romagnoli, M. Moshin, M. Otto, D. Neumaier, I. Asselberghs, J. Van Campenhout, and C. Huyghebaert, "Complex effective index in graphene-silicon waveguides," Optics Express, vol. 24, no. 26, pp. 29984–29993, Dec. 2016.

[5] T. Otsuji, S. B. Tombet, A. Satou, M. Ryzhii, and V. Ryzhii, "Terahertz-wave generation using graphene: Toward new types of terahertz lasers," IEEE Journal of Selected Topics in Quantum Electronics, vol. 19, no. 1, p. 8400209, Jul. 2012.

[6] J. Gosciniak, D. Tan, and B. Corbett, "Enhanced performance of graphene-based electro-absorption waveguide modulators by engineered optical modes," Journal of Physics D: Applied Physics, vol. 48, no. 23, p. 235101, May 2015.

[7] X. Hu and J. Wang, "High Figure of Merit Graphene Modulator Based on Long-Range Hybrid Plasmonic Slot Waveguide," IEEE Journal of Quantum Electronics, vol. 53, no. 3, p. 7200308, Jun. 2017.

[8] M. Midrio, S. Boscolo, M. Moresco, M. Romagnoli, C. De Angelis, A. Locatelli, and A.-D. Capobianco, "Graphene–assisted critically–coupled optical ring modulator," Optics Express, vol. 20, no. 21, pp. 23144–23155, Oct. 2012.

[9] S. Ye, Z. Wang, L. Tang, Y. Zhang, R. Lu, and Y. Liu, "Electro-absorption optical modulator using dual-graphene-on-graphene configuration," Optics Express, vol. 22, no. 21, pp. 26173–26180, Oct. 2014.

[10] M. M. Jadidi, A. B. Sushkov, R. L. Myers-Ward, A. K. Boyd, K. M. Daniels, D. K. Gaskill, M. S. Fuhrer, H. D. Drew, and T. E. Murphy, "Tunable terahertz hybrid metal–graphene plasmons," Nano Letters, vol. 15, no. 10, pp. 7099–7104, Sep. 2015.

[11] E. S. Torabi, A. Fallahi, and A. Yahaghi, "Evolutionary Optimization of Graphene-Metal Metasurfaces for Tunable Broadband Terahertz Absorption," IEEE Transactions on Antennas and Propagation, vol. 65, no. 3, pp. 1464–1467, Mar. 2017.

[12] Y. S. Cao, L. J. Jiang, and A. E. Ruehli, "An equivalent circuit model for graphene-based terahertz antenna using the PEEC method," IEEE Transactions on Antennas and Propagation, vol. 64, no. 4, pp. 1385–1393, Apr. 2016.

[13] W. Fuscaldo, P. Burghignoli, P. Baccarelli, and A. Galli, "Graphene Fabry–Perot Cavity Leaky-Wave Antennas: Plasmonic Versus Nonplasmonic Solutions," IEEE Transactions on Antennas and Propagation, vol. 65, no. 4, pp. 1651–1660, Apr. 2017.

[14] J. M. Jornet and I. F. Akyildiz, "Graphene-based plasmonic nano-antenna for terahertz band communication in nanonetworks," IEEE Journal on Selected Areas in Communications, vol. 31, no. 12, pp. 685–694, Dec. 2013.

[15] M. N. Moghadasi, R. A. Sadeghzadeh, M. Toolabi, P. Jahangiri, and F. B. Zarrabi, "Fractal cross aperture nano-antenna with graphene coat for bio-sensing application," Microelectronic Engineering, vol. 162, pp. 1–5, Apr. 2016.

[16] A. Locatelli, G. E. Town, and C. De Angelis, "Graphene-based terahertz waveguide modulators," IEEE Transactions on Terahertz Science and Technology, vol. 5, no. 3, pp. 351–357, May 2015.

[17] B. Xiao, R. Sun, J. He, K. Qin, S. Kong, J. Chen, and W. Xiumin, "A Terahertz Modulator Based on Graphene Plasmonic Waveguide," IEEE Photonics Technology Letters, vol. 27, no. 20, pp. 2190–2192, Oct. 2015.

[18] Z. Chang, B. You, L.-S. Wu, M. Tang, Y.-P. Zhang, and J.-F. Mao, "A reconfigurable graphene reflectarray for generation of vortex THz waves," IEEE Antennas and Wireless Propagation Letters, vol. 15, pp. 1537–1540, Jan. 2016.

[19] A. Tredicucci and M. S. Vitiello, "Device concepts for graphene-based terahertz photonics," IEEE Journal of Selected Topics in Quantum Electronics, vol. 20, no. 1, p. 8500109, Jul. 2014.

[20] C. Han and I. F. Akyildiz, "Three-Dimensional End-to-End Modeling and Analysis for Graphene-Enabled Terahertz Band Communications," IEEE Transactions on Vehicular Technology, no. 99, Sep. 2016.

[21] K. Sugawara, T. Kawasaki, G. Tamamushi, H. Mastura, A. Dobroiu, T. Yoshida, T. Suemitsu, H. Fukidome, M. Suemitsu, V. Ryzhii, K. Iwatsuki, S. Kuwano, J.-I. Kani, T. Jun, and T. Otsuji, "Photonic Frequency Double-Mixing Conversion Over the 120-GHz Band Using InP-and Graphene-Based Transistors," IEEE Journal of Lightwave Technology, vol. 34, no. 8, pp. 2011–2019, Apr. 2016.

[22] Q. H. Abbasi, K. Yang, N. Chopra, J. M. Jornet, N. A. Abuali, K. A. Qaraqe, and A. Alomainy, "Nano-Communication for Biomedical Applications: A Review on the State-of-the-Art From Physical Layers to Novel Networking Concepts," IEEE Access, vol. 4, pp. 3920–3935, Jul. 2016.

[23] M. Aidi, M. Hajji, A. Ben Ammar, and T. Aguili, "Graphene nanoribbon antenna modeling based on MoM-GEC method for electromagnetic nanocommunications in the terahertz range," Journal of Electromagnetic Waves and Applications, vol. 30, no. 8, pp. 1032–1048, May 2016.

[24] A. Tsioliaridou, C. Liaskos, S. Ioannidis, and A. Pitsillides, "Lightweight, self-tuning data dissemination for dense nanonetworks," Nano Communication Networks, vol. 8, pp. 2–15, Jun. 2016.

[25] T. Stauber, N. Peres, and A. Geim, "Optical conductivity of graphene in the visible region of the spectrum," Physical Review B, vol. 78, no. 8, p. 085432, Aug. 2008.

[26] X. Chen, Y. Wang, Y. Xiang, G. Jiang, L. Wang, Q. Bao, H. Zhang, Y. Liu, S. Wen, and D. Fan, "A Broadband Optical Modulator Based on a Graphene Hybrid Plasmonic Waveguide," IEEE Journal of Lightwave Technology, vol. 34, no. 21, pp. 4948–4953, Nov. 2016.

[27] D. Pérez, D. Domenech, P. Muñoz, and J. Capmany, "Electro-Refraction Modulation Predictions for Silicon Graphene Waveguides in the 1540–1560 nm Region," IEEE Photonics Journal, vol. 8, no. 5, p. 4501613, Oct. 2016.

[28] S.-W. Ye, F. Yuan, X.-H. Zou, M. K. Shah, R.-G. Lu, and Y. Liu, "High-speed optical phase modulator based on graphene-silicon waveguide," IEEE Journal of Selected Topics in Quantum Electronics, vol. 23, no. 1, p. 3400105, Mar. 2017.

[29] A. Andryieuski and A. V. Lavrinenko, "Graphene metamaterials based tunable terahertz absorber: effective surface conductivity approach," Optics Express, vol. 21, no. 7, pp. 9144–9155, Apr. 2013.

[30] B. Sensale-Rodriguez, R. Yan, L. Liu, D. Jena, and H. G. Xing, "Graphene for reconfigurable terahertz

optoelectronics," Proceedings of the IEEE, vol. 101, no. 7, pp. 1705–1716, Jul. 2013.

[31] G. Yao, F. Ling, J. Yue, Q. Luo, and J. Yao, "Dynamically Tunable Graphene Plasmon-Induced Transparency in the Terahertz Region," IEEE Journal of Lightwave Technology, vol. 34, no. 16, pp. 3937–3942, Aug. 2016.

[32] S. Bahadori-Haghighi, R. Ghayour, and M. H. Sheikhi, "Three-Dimensional Analysis of an Ultrashort Optical Cross-Bar Switch Based on a Graphene Plasmonic Coupler," IEEE Journal of Lightwave Technology, vol. 35, no. 11, pp. 2211–2217, Jun. 2017.

[33] I. Llatser, C. Kremers, A. Cabellos-Aparicio, J. M. Jornet, E. Alarcón, and D. N. Chigrin, "Graphene-based nano-patch antenna for terahertz radiation," Photonics and Nanostructures-Fundamentals and Applications, vol. 10, no. 4, pp. 353–358, Oct. 2012.

[34] X. Zhou, T. Zhang, X. Yin, L. Chen, and X. Li, "Dynamically Tunable Electromagnetically Induced Transparency in Graphene-Based Coupled Micro-Ring Resonators," IEEE Photonics Journal, vol. 9, no. 2, Apr. 2017.

[35] M. A. Vozmediano, "Renormalization group aspects of graphene," Philosophical Transactions of the Royal Society of London A: Mathematical, Physical and Engineering Sciences, vol. 369, no. 1946, pp. 2625–2642, Jun. 2011.

[36] J. Capmany, D. Doménech, and P. Muñoz, "Graphene integrated microwave photonics," IEEE Journal of Lightwave Technology, vol. 32, no. 20, pp. 3785–3796, Oct. 2014.